Synopsis of Ph.D. thesis:

Thesis title:

# Electronic Structure of Correlated electrons

Proposed to be submitted towards
partial fulfillment of the degree of
**Doctor of Philosophy**
**of**
**PRESIDENCY UNIVERSITY**


**Candidate: Manoj Gupta**

Department of Condensed Matter and Material Physics
S. N. Bose National Centre for Basic Sciences,
Block-JD, Sector-III, Salt Lake, Kolkata-700106, INDIA

**Supervisor: Prof. Tanusri Saha-Dasgupta**

Department of Condensed Matter and Material Physics
S. N. Bose National Centre for Basic Sciences,
Block-JD, Sector-III, Salt Lake, Kolkata-700106, INDIA


**Signature of the Candidate:**

**Signature of Supervisor:**

# Acknowledgement

I take this opportunity to express my deepest sense of gratitude and sincere thanks to everyone who helped me complete the work successfully.

First and foremost, I would like to express my sincere gratitude to my supervisor, **Prof. Tanusri Saha-Dasgupta**, Department of **Condensed Matter and Material Physics**, **SNBNCBS**, for her unwavering support and guidance throughout the project. Her insights and encouragement have been invaluable.

I would also like to acknowledge the contributions of my collaborators and coauthors **Dr. Basudeb Mondal**, **Mr. Manodip Routh**, and **Dr. Arun Kumar Maurya** for their expertise and inputs which significantly enhanced the quality of works in various projects.

Additionally, I am grateful to **Prof. Subhro Bhattacharjee**, **Prof. Manoranjan Kumar**, and **Prof. Arijit Haldar** for their valuable guidance, feedback and suggestions that were instrumental in the various projects.

Finally, I thank my parents, family and friends for their continuous support and encouragement throughout this journey.

**Manoj Gupta**

## Talks and Conferences Attended

- **Oral Presentation**, *BOSE-FEST 2025*, the annual in-house scientific talk and poster presentation event at SNBNCBS, Kolkata, India. (Feb 2025)
- **Poster Presentation**, *International Conference on Bose-Einstein Condensation, Superconductivity, Superfluidity and Quantum Magnetism (ICBEC-2024)*, SNBNCBS, Kolkata, India. (Nov 2024)
- **Oral Presentation**, *BOSE-FEST 2024*, the annual in-house scientific talk and poster presentation event at SNBNCBS, Kolkata, India. (Feb 2024)
- **Poster Presentation**, *International Conference on Highly Frustrated Magnetism (HFM 2024)*, IIT Madras, Chennai, India. (Jan 2024)
- **Poster Presentation**, *Annual Conference on Quantum Condensed Matter (QMAT-2023)*, NISER, Bhubaneswar, India. (Nov 2023)
- **Poster Presentation**, *BOSE-FEST 2023*, the annual in-house scientific talk and poster presentation event at SNBNCBS, Kolkata, India. (Feb 2023)
- **Second Academic Visit**, *International Centre for Theoretical Sciences (ICTS)*, Bangalore, India, for collaborative research discussions. (5th–13th November 2023)
- **First Academic Visit**, *International Centre for Theoretical Sciences (ICTS)*, Bangalore, India, for collaborative research. (23rd–31st January 2023)
- **Poster Presentation**, *CCQM-22*, jointly organized by APCTP, IACS, and SNBNCBS at SNBNCBS, Kolkata, India. (17th–25th November 2022)

# List of Publications

1. **Manoj Gupta**, Basudeb Mondal, Subhro Bhattacharjee, Tanusri Saha-Dasgupta,
   *"Ab initio insights on the fermiology of $d^1$ transition metals on the honeycomb lattice: Hierarchy of hopping pathways and spin-orbit coupling"*, Phys. Rev. Research **5**, 043219 (2023).

2. **Manoj Gupta**, Arijit Haldar, Subhro Bhattacharjee, Tanusri Saha-Dasgupta,
   *"Multiple Dirac Spin-Orbital Liquids for SU(4) Heisenberg Antiferromagnets on Honeycomb Lattice"*, cond-mat.str-el: arXiv.2508.18372.

3. **Manoj Gupta**, Manodip Routh, Manoranjan Kumar, Tanusri Saha-Dasgupta,
   *"Interchain interactions, multimagnon condensation, and strain effect in the chain compound $NaVOPO_4$"*, Phys. Rev. B **110**, 054441 (2024).

4. **Manoj Gupta**, Arun Kumar Maurya, Amal Medhi, Tanusri Saha-Dasgupta,
   *"Role of topotactic hydrogen in Superconductivity of Infinite-layer Nickelate $NdNiO_2$: A first-principles and variational Monte Carlo study"*, cond-mat.supr-con: arXiv:2506.13399

# Contents


**Title** i

**Acknowledgments** i

**Talks and Conferences Attended** iii

**Talks and Conferences Attended** iii

**Synopsis** 1

**1 General Introduction** 1

**2 Emergent Quantum Phenomena from the Interplay of Correlation ($U$) and Spin-Orbit Coupling ($\lambda$)** 2

2.1 Electronic Band Theory and Crystal Field Splitting in Weakly Correlated Solids . . . 3

2.2 High-$T_c$ Superconductors . . . 4

2.3 Low-Energy Magnets . . . 5

2.4 Spin-Orbital Liquid . . . 5

**3 Methodology** 6

3.1 Density Functional Theory(DFT) . . . 6

3.2 Parton Construction and Mean-Field Theory of Quantum Spin Liquids . . . 7

3.3 Exact Diagonalization(ED) and Density Matrix Renormalization (DMRG) . . . 8

3.3.1 ED . . . 8

3.3.2 DMRG . . . 9

3.4 Variational Monte Carlo . . . 9

**4 Results** 10

4.1 Project-I: Ab initio insights on the fermiology of $d^1$ transition metals on the honeycomb lattice: Hierarchy of hopping pathways and spin-orbit coupling . . . 10

4.2 Project-II: Multiple Dirac Spin-Orbital Liquids for SU(4) Heisenberg Antiferromagnets on Honeycomb Lattice . . . 12

4.3 Project-III: Interchain Interactions and Multimagnon Condensation in $NaVOPO_4$ . . . 15

4.4 Project-IV: Role of topotactic hydrogen in Superconductivity of Infinite-layer Nickelate NdNiO2: A first-principles and variational Monte Carlo study . . . 17

**Bibliography** 19

# 1 General Introduction

Correlated electron systems have emerged as a central topic in condensed matter physics due to the wide variety of exotic quantum phases that they can exhibit. Particularly, transition-metal compounds with partially filled $3d$, $4d$, and $5d$ shells demonstrate the interplay among charge, spin, and orbital degrees of freedom. This interplay is often governed by an accidental balance between electron-electron interactions and crystal field splitting [1, 2]. Depending on the relative strengths of these effects, a wide range of quantum states such as Mott insulators, unconventional low-energy magnets, high-temperature superconductors and spin-orbital liquid can appear [3, 4].

Spin-Orbital Coupling(SOC) is an important ingredient in understanding the behavior of heavier transition-metal systems. SOC originates from relativistic effects, where an electron's spin couples to its orbital motion. Although, generally, weak in lighter elements, SOC increases significantly in heavier atoms, scaling roughly as $Z^4$ with the atomic number $Z$. This enhanced SOC, can lift orbital degeneracies and significantly modify the electronic structure, especially when combined with moderate or strong electronic correlations. In weakly correlated systems, SOC has already led to the discovery of topological insulators and Weyl semimetals [5–7]. However, in systems where electron-electron interactions are strong, it can be quantified by the Hubbard $U$ that penalizes double occupancy. Further, SOC can introduce entirely new physics [8]. It can give rise to spin-orbit entangled local moments that do not follow conventional spin or orbital classification. The collective behavior of these entangled moments can lead to unconventional magnetic orders, spin liquids, and nontrivial superconducting phases. The emergence of such complex behavior in correlated systems with strong SOC has motivated extensive theoretical and experimental investigations. To capture the essence of these competing interactions, a minimal model Hamiltonian is given by:

$$H = \sum_{i,j;\alpha,\beta} t_{ij,\alpha\beta} c^{\dagger}_{i\alpha} c_{j\beta} + \text{h.c.} + \lambda \sum_{i} \mathbf{L}_i \cdot \mathbf{S}_i + U \sum_{i,\alpha} n_{i\alpha}(n_{i\alpha} - 1), \tag{1.1}$$

where $t_{ij,\alpha\beta}$ is the hopping amplitude between orbitals $\alpha$ and $\beta$ on sites $i$ and $j$, $\lambda$ is the strength of atomic SOC, and $U$ is the on-site Coulomb repulsion. Here, $c_{i\alpha}$ annihilates an electron in orbital $\alpha$ at site $i$, and $n_{i\alpha} = c^{\dagger}_{i\alpha} c_{i\alpha}$ is the corresponding occupation number. The model neglects Hund's coupling for simplicity, though it can play an important role in multi-orbital systems.

Figure 1 shows a schematic phase diagram based on this model, plotted in the space of $U/t$ (vertical axis) and $\lambda/t$ (horizontal axis), where $t$ represents the characteristic hopping strength [10]. The diagram illustrates four primary regimes separated by crossover lines: weakly and strongly correlated, and weakly and strongly spin-orbit coupled. On the left side of the diagram (low $\lambda/t$), conventional $3d$ transition-metal compounds lie, where SOC is negligible and Mott transitions are governed solely by $U$. As one increases $\lambda$ while keeping $U$ small, topological insulators and semimetals emerge. On the other hand, for large $U$, Mott localization suppresses kinetic energy, enhancing the relative importance of SOC. This can lead to new magnetic ground states or even quantum spin-orbital liquids [11–13]. In the intermediate regime where both $U$ and $\lambda$ are comparable to $t$, SOC and correlations mutually reinforce each other. For instance, SOC can lift orbital degeneracies and reduce the bandwidth, thus lowering the critical $U$ required for Mott transitions. In turn, Mott localization enhances SOC effects by suppressing electronic motion, thereby reducing the energy scale of magnetic exchange $J \sim t^2/U$. As a result, the competition in this regime is effectively between SOC and $J$, not just $\lambda$ and $U$ directly. This interdependence shifts the crossover boundaries within the phase diagram and leads to a wealth of novel phases.

A number of material systems are now known to fall in this correlated SOC regime. Notably, iridates such as $(Na/Li)_2IrO_3$ [14], $RuCl_3$ [15], and $ZrCl_3$ [16] have caught significant attention. These systems are often Mott insulators despite their extended $5d$ orbitals, primarily due to the combined effect of moderate $U$ and strong SOC ($\lambda \approx 0.4$ eV). Other relevant systems include pyrochlore iridates ($R_2Ir_2O_7$) [17], osmates like $NaOsO_3$ [18]

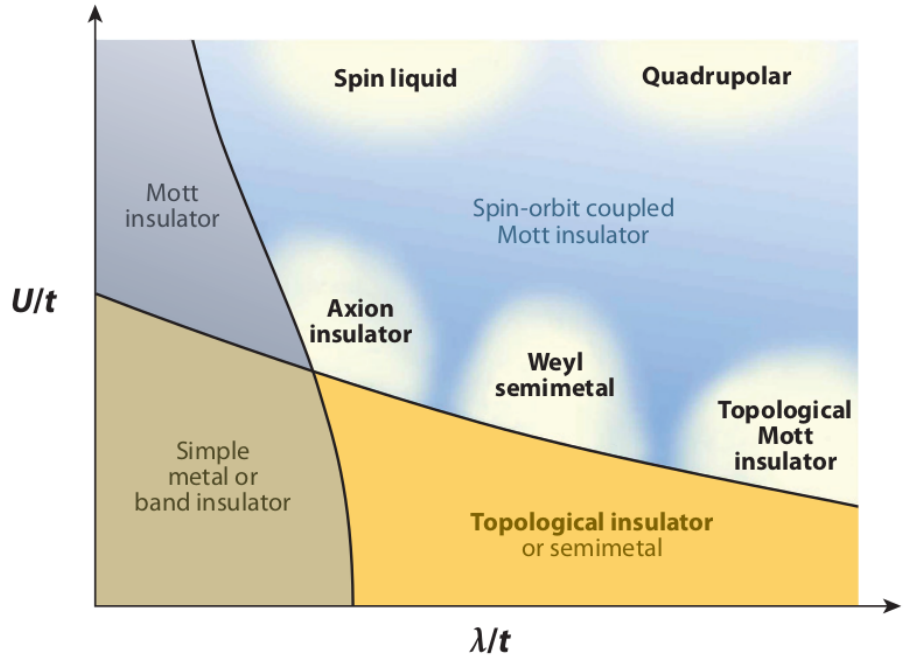


**Figure 1:** *General form of the phase diagram in the presence of electronic-correlations and spin-orbit coupling. Figure adapted from the review [9]*

and $Cd_2Os_2O_7$ [19], and spinel-derived materials. Some vanadates such as $Sr_2VO_4$ [20], and spin-orbit liquid candidates like $FeSc_2S_4$ [21], reside at the upper end of the diagram, where magnetic exchange is suppressed and SOC dominates.

In conclusion, the interplay of electronic correlation and spin-orbit coupling in transition-metal compounds continues to uncover new ground states and phenomena. Understanding these effects within minimal theoretical models and comparing with material-specific calculations remains a vibrant area of research in modern condensed matter physics.

## 2 Emergent Quantum Phenomena from the Interplay of Correlation ($U$) and Spin-Orbit Coupling ($\lambda$)

This thesis explores the diverse quantum phases and emergent phenomena that arise from the interplay between electron-electron interaction strength ($U$) and spin-orbit coupling ($\lambda$), effectively navigating through different regimes of the $U$–$\lambda$ phase diagram.

In the **first project**, we investigated systems characterized by strong spin-orbit coupling ($\lambda$) but weak electronic correlation ($U \ll t$). The focus was on understanding how the electronic structure and Fermi surface topology of $\alpha$-$ZrCl_3$ evolve due to the hierarchy of hopping pathways in the presence of significant SOC. Using downfolding and tight-binding methods, we demonstrated that even in the absence of strong Coulomb interactions, SOC can lead to rich orbital textures and nontrivial band reconstructions. In this regime, electronic correlations were treated perturbatively or neglected altogether, as the primary qualitative features were governed by SOC and band topology.

The **second project** delves into the opposite corner of the phase diagram, where both electronic correlations and spin-orbit coupling are strong ($U \gg t$, $\lambda \sim t$). Here, we examined the emergence of spin-orbital entan-

gled states and the possible realization of exotic quantum phases such as spin-orbital liquids in $\alpha$-$ZrCl_3$-inspired models. Utilizing perturbative expansion techniques and effective spin models derived from the onsite-Hubbard models, we captured the physics of strongly interacting electrons in the presence of entangled spin and orbital degrees of freedom. This project reveals how the cooperative effect of $U$ and $\lambda$ can give rise to fundamentally new low-energy fractionalized excitations and ground states that are inaccessible in either limit alone.

In contrast, the **third and fourth projects** investigate systems with strong Coulomb interactions ($U \gg t$) but relatively weak spin-orbit coupling ($\lambda \ll t$). In these limits, spin-orbit effects act as small perturbations, while the dominant physics is governed by electron correlation and exchange mechanisms. In the third project, we studied low-dimensional spin systems and the emergence of quantum magnetism, including phenomena such as spin gaps, and Bose-Einstein condensation in alternating spin-$1/2$ chains for $NaVOPO_4$. In the fourth project, we explored unconventional superconductivity in correlated system such as infinite-layer Nickelate $NdNiO_2$, focusing on high-$T_c$ superconductors where the Mott insulating state and spin fluctuations play a critical role in the pairing mechanism. These projects emphasize the rich landscape of emergent low-energy physics driven primarily by strong correlations and SOC.

Together, these four projects systematically explore the four quadrants of the $U$–$\lambda$ parameter space(c.f Fig 1), highlighting how distinct physical mechanisms dominate in different regimes. The findings illustrate the versatility of theoretical models and computational techniques in capturing the complex behavior of correlated electron systems across this multidimensional phase space.

## 2.1 Electronic Band Theory and Crystal Field Splitting in Weakly Correlated Solids

In weakly correlated materials, the on-site Coulomb repulsion ($U$) is much smaller than the electronic bandwidth ($t$), i.e., $U/t \ll 1$. This is attributed to the effective screening of electron-electron coloumbic interaction due to the core electrons minimizing the electronic correlations. It allows their effects to be captured through perturbative or mean-field approaches [22]. Consequently, the electronic structure of such systems is well described using single-particle theories such as the tight-binding approximation, free-electron models, and density functional theory (DFT) with exchange-correlation functionals like the Local Density Approximation (LDA) [23] and the Generalized Gradient Approximation (GGA) [24].

The central framework for understanding the electronic structure in such solids is provided by band theory [25, 26]. At large interatomic distances, atoms contribute discrete electronic states, which are degenerate across lattice sites. As atoms come closer to form a periodic crystal lattice, quantum mechanical overlap between atomic orbitals leads to the formation of energy bands. This phenomenon was rigorously formalized by Bloch, who demonstrated that electronic wavefunctions in a periodic potential take the form:

$$\psi_{n\mathbf{k}}(\mathbf{r}) = e^{i\mathbf{k}\cdot\mathbf{r}} u_{n\mathbf{k}}(\mathbf{r}),$$

where $u_{n\mathbf{k}}(\mathbf{r})$ has the periodicity of the crystal lattice. The allowed energy levels form bands $E_n(\mathbf{k})$ that vary continuously with crystal momentum $\mathbf{k}$.

The band structure emerges from solving the Schrödinger equation in the presence of a periodic potential:

$$V(\mathbf{r}) = \sum_j u_a(\mathbf{r} - \mathbf{R}_j),$$

where $u_a$ is the atomic potential at site $\mathbf{R}_j$. At large separations, the energy levels $\varepsilon_\alpha$ are $N$-fold degenerate for a system of $N$ atoms. With decreasing lattice spacing, this degeneracy is lifted due to hybridization, resulting in the formation of dispersive bands whose bandwidth reflects the hopping strength between orbitals.

An additional feature that shapes the band structure, especially in transition metal compounds, is *crystal field*

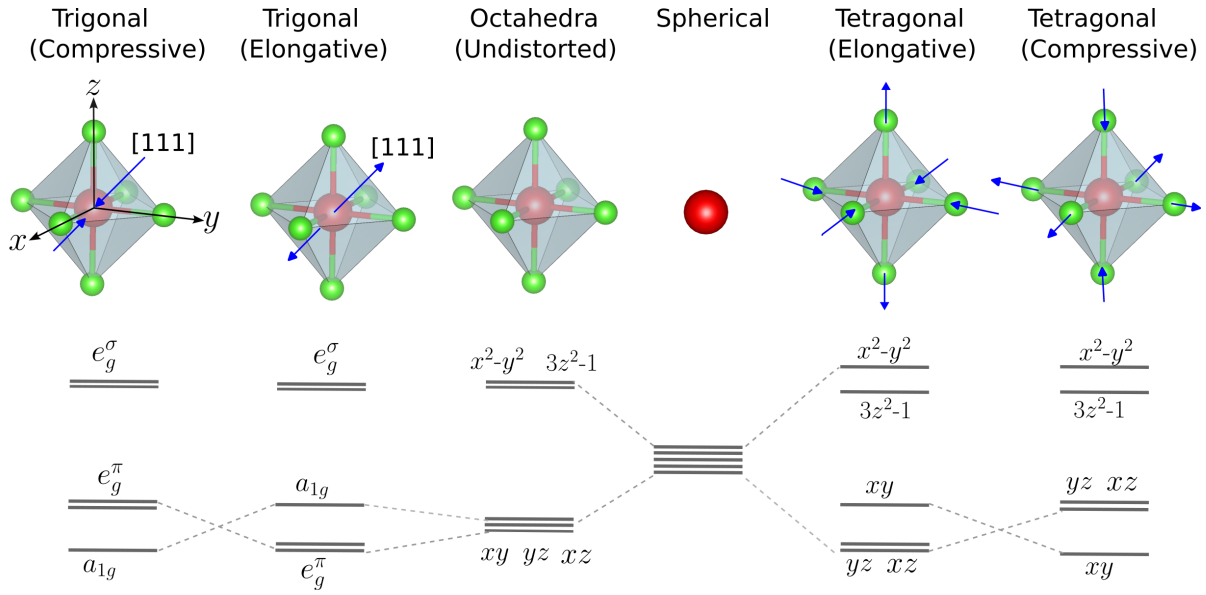


**Figure 2:** *Schematic illustration of crystal field splitting in spherical, cubic, tetragonal, and trigonal environments.*

*splitting* [27, 28]. In free atoms, $d$-orbitals are degenerate due to spherical symmetry. However, when an atom is embedded in a crystal environment, this symmetry is reduced by surrounding ions (ligands), leading to a lifting of the orbital degeneracy. For example, in an octahedral coordination common in perovskites, the fivefold-degenerate $d$ orbitals split into two groups: a lower-energy $t_{2g}$ triplet ($d_{xy}, d_{yz}, d_{xz}$) and a higher-energy $e_g$ doublet ($d_{x^2-y^2}, d_{3z^2-r^2}$). This crystal field splitting modifies the orbital character of the bands and influences the occupation of electronic states near the Fermi level.

Further distortions from ideal symmetry, such as tetragonal or trigonal distortions [c.f. Fig 2], can lead to additional splitting of $t_{2g}$ or $e_g$ levels, shaping the low-energy electronic landscape. In weakly correlated compounds, such crystal field effects are accurately captured within DFT calculations and play a crucial role in determining electronic, magnetic, and orbital properties.

Thus, in weakly correlated solids, the interplay of band formation and crystal field effects governs the overall electronic structure, enabling a robust description of metallicity, semiconducting gaps, and orbital ordering phenomena.

## 2.2 High-$T_c$ Superconductors

Conventional superconductivity, described by BCS theory [29], arises from electron-phonon coupling and Cooper pairing, leading to a zero-resistance state below a critical temperature $T_c$. In contrast, high-$T_c$ superconductivity, first discovered in 1986 in the cuprate $La_{2-x}Ba_xCuO_4$ [30], cannot be explained by Fermi-liquid theory. Cuprates are layered perovskite oxides with $CuO_2$ planes, and their parent compounds (such as, $La_2CuO_4$ [31] and $YBa_2Cu_3O_{6+y}$ [32]) are antiferromagnetic Mott insulators with $Cu^{2+}$ in a $d^9$ configuration. Hole doping (such as via Sr or Ba substitution) introduces carriers into the $CuO_2$ planes, suppressing magnetism and inducing superconductivity. The superconducting dome typically appears between 5–25% hole concentration, with $T_c$ peaking around 40 K in $La_{2-x}Sr_xCuO_4$ and reaching up to 93 K in $YBa_2Cu_3O_{6+y}$.

Nickelates, such as $Nd_{1-x}Sr_xNiO_2$ [33], have recently emerged as cuprate analogs due to their $Ni^{1+}$ ($d^9$) state. Superconductivity in infinite-layer nickelates was discovered in 2019, following attempts in systems like $LaNiO_3$ superlattices and trilayers ($La_3Ni_2O_6$ [34], $La_4Ni_3O_8$ [35]). Unlike cuprates, the undoped nickelates are weakly metallic. A narrower superconducting dome ($0.125 < x < 0.25$) [36] appears with Sr doping, accompanied by unusual transport signatures, including resistivity upturns. These materials present a new platform to explore

unconventional superconductivity beyond cuprates.

## 2.3 Low-Energy Magnets

Low-dimensional quantum magnets provide an excellent platform for exploring the interplay between strong correlations and quantum fluctuations. In systems described by the effective Heisenberg Hamiltonian (2.1), especially in one and two dimensions with low spin values ($S = 1/2$, $S = 1$), conventional long-range magnetic order is strongly suppressed by quantum effects, often leading to exotic ground states and excitation spectra.

$$H = \frac{4t^2}{U} \sum_{\langle ij \rangle} \mathbf{S}_i \cdot \mathbf{S}_j = J \sum_{\langle ij \rangle} \mathbf{S}_i \cdot \mathbf{S}_j, \tag{2.1}$$

Historically, the 1D Ising model [37] introduced in 1925 revealed the absence of spontaneous magnetization at finite temperatures. Its isotropic counterpart, the Heisenberg model [38] includes spin-spin interactions in all directions and remains disordered at any non-zero temperature in 1D and 2D due to the *Mermin-Wagner theorem* [39]. Nevertheless, magnetic ordering can still arise in the presence of anisotropy or inter-layer coupling.

An essential distinction exists between integer and half-integer uniform spin chains. While $S = 1/2$ systems are gapless and host fractionalized excitations, $S = 1$ systems exhibit a *Haldane gap* [40], a finite energy gap $\Delta$ between the ground and first excited states. Further dimerization in the spin-chain $S = 1/2$ can also results in spin-gaps. This gap suppresses low-energy magnetic excitations, reflected experimentally by an exponential drop in magnetic susceptibility $\chi(T) \sim e^{-\Delta/k_B T}$ at low temperatures.

Several materials exhibit such spin-gapped behavior:

- $CuTe_2O_5$ [41]: Contains $S = 1/2$ dimers formed from edge-sharing $CuO_6$ octahedra. Magnetic susceptibility peaks at $T = 56$ K and declines rapidly, indicating $J \approx 90$ K.
- $CsV_2O_5$ [42]: Features alternating magnetic $V^{4+}$ and nonmagnetic $V^{5+}$ ions forming weakly coupled dimers. A significant spin gap $\Delta = 146$ K arises due to alternating exchange.
- $CuGeO_3$ [43]: Undergoes a spin-Peierls transition marked by lattice dimerization and a $\lambda$-type anomaly in specific heat.

A remarkable phenomenon in some of these low-dimensional magnets is the realization of *Bose-Einstein condensation* (BEC) [44] of magnons under applied magnetic fields. In dimerized or gapped systems, an external magnetic field splits the triplet excitation levels, lowering the $S_z = +1$ state. Once the gap closes at a critical field $H_{c1}$, a condensate of triplet excitations forms, leading to a field-induced antiferromagnetic order. The phase boundary near $H_{c1}$ follows the power law $H_{c1}(T) - H_{c1}(0) \propto T^{3/2}$, characteristic of BEC in three dimensions. Materials such as $BaCuSi_2O_6$ [45], $Ba_3Mn_2O_8$ [46], and $NiCl_2 - 4SC(NH_2)_2$ [47] exhibit such field-induced BEC phases, with rich phase diagrams identified by anomalies in magnetization and specific heat.

These systems bridge condensed matter and quantum statistical physics, providing tunable platforms for studying many-body bosonic condensation and quantum phase transitions in solid-state systems.

## 2.4 Spin-Orbital Liquid

The interplay of spin-orbit coupling (SOC) and electron-electron interactions has emerged as a powerful route to realizing novel phases of correlated quantum matter. In particular, spin-orbit coupled Mott insulators have garnered widespread attention for their ability to host frustrated magnetic interactions that arise naturally due to the entanglement of spin and orbital degrees of freedom. Such frustration suppresses classical magnetic ordering and opens up the possibility of realizing quantum paramagnetic phases, including various forms of quantum spin

liquids (QSLs) [3, 11]. Prime examples of such systems include Kitaev materials and spin-ice compounds [14, 48–50], where bond-dependent anisotropic interactions are direct manifestations of strong SOC and crystal field effects.

Two essential features define these SOC-assisted magnetic systems: (1) the emergence of spin-orbitally entangled effective spin-$1/2$ degrees of freedom, and (2) the explicit breaking of SU(2) spin-rotation symmetry down to discrete subgroups due to the intertwining of spin and lattice symmetries. These features result in highly anisotropic exchange interactions that often defy traditional Heisenberg-type descriptions.

In a seminal work, Yamada *et al.* [13] studied the Hubbard model for quarter-filled $J = 3/2$ electrons on the honeycomb lattice, motivated by trihalide compounds such as $\alpha$-$ZrCl_3$. They demonstrated that when indirect, symmetry-allowed nearest-neighbor hopping pathways are combined with strong onsite Coulomb repulsion, the resulting low-energy model exhibits an emergent SU(4) symmetry. This enhanced symmetry arises after performing a site-dependent rotation of the $J = 3/2$ orbitals, effectively mapping the model to an SU(4) antiferromagnetic Heisenberg Hamiltonian.

Remarkably, SU(4) spin models have long been proposed to support exotic QSL ground states. Earlier analytical work by Affleck, Marston and Read et. al. [51] demonstrated that in the large-$N$ limit, SU($N$) antiferromagnets on bipartite lattices can stabilize nontrivial QSLs. Recent numerical studies [**?**] support this scenario, indicating that the SU(4) Heisenberg model on the honeycomb lattice favors a gapless U(1) Dirac spin liquid as its ground state.

The implications for spin-orbit coupled trihalide materials are profound. If the conditions for emergent SU(4) symmetry are met, these compounds could realize a quantum spin-orbital liquid (QSOL) phase with Dirac-like low-energy excitations, referred to as a Dirac quantum spin-orbital liquid (DQSOL), making them highly promising platforms for exploring new regimes of quantum entanglement and fractionalization.

# 3 Methodology

## 3.1 Density Functional Theory(DFT)

Solving the many-electron Schrödinger equation exactly is extremely difficult due to the complexity introduced by interactions between electrons. Density Functional Theory (DFT), introduced by Hohenberg and Kohn in 1964 [52], offers a powerful way to simplify this problem. Instead of working with the complicated many-electron wavefunction, DFT uses the electron density $n(\mathbf{r})$ as the main quantity. Their theorems show that the ground state properties of a system are completely determined by its electron density and that the ground state energy is obtained by minimizing an energy functional $E[n]$ with respect to this density.

However, these theorems did not explain how to construct the energy functional in practice. This challenge was addressed in 1965 by Kohn and Sham [23], who proposed a method where the real interacting system is replaced with a system of non-interacting electrons moving in an effective potential. These electrons obey the so-called Kohn-Sham equations:

$$\left[-\frac{\hbar^2}{2m}\nabla^2 + V_{\text{ext}}(\mathbf{r}) + V_{\text{H}}(\mathbf{r}) + V_{\text{xc}}(\mathbf{r})\right]\phi_i(\mathbf{r}) = \varepsilon_i\phi_i(\mathbf{r}). \tag{3.1}$$

Here, $V_{\text{ext}}$ is the potential from the nuclei, $V_{\text{H}}$ accounts for the classical repulsion between electrons, and $V_{\text{xc}}$ represents the more complicated exchange and correlation effects. The total energy of the system is given by:

$$E[n] = T_s[n] + J[n] + E_{\text{xc}}[n] + \int V_{\text{ext}}(\mathbf{r})n(\mathbf{r})\,d^3r, \tag{3.2}$$

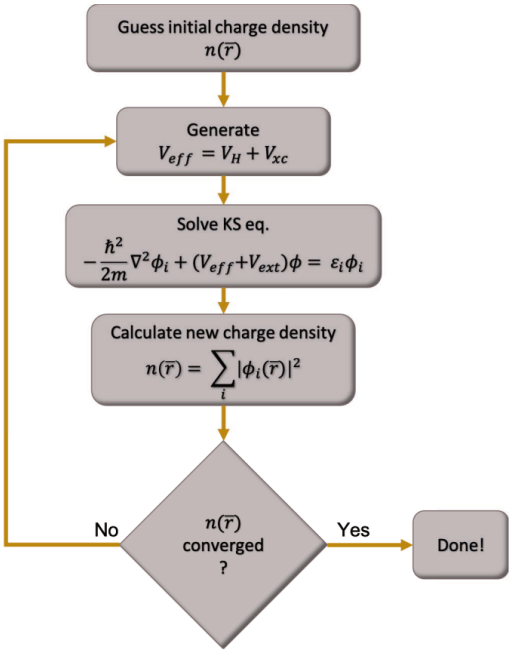


**Figure 3:** *Flowchart of the self-consistent KS-DFT method.*

where $T_s[n]$ is the kinetic energy of non-interacting electrons and $J[n]$ is the classical electron-electron repulsion energy.

The self-consistent method of generating the ground state density is outlined in Fig 3. Starting with an initial guess for the Kohn-Sham orbitals, or the electron density, one can solve the Kohn-Sham equations Eq (3.1) and obtain a new set of Kohn-Sham orbitals that generate a new electron density. By repeating this process until the density used in Kohn-Sham density functional theory equations differs from the density obtained from the new Kohn-Sham by no more than a predetermined numerical convergence limit.

Since the exact form of the exchange-correlation energy $E_{\text{xc}}$ is unknown, it must be approximated. The simplest approximation is the Local Density Approximation (LDA) [23], which assumes the energy depends only on the local value of the density. A more accurate approach is the Generalized Gradient Approximation (GGA), which also includes how the density changes in space. One widely used GGA functional is PBE [24].

To go even further, meta-GGA functionals include additional information such as the kinetic energy density. A popular example is the SCAN functional [53], which works well for both molecules and solids.

## 3.2 Parton Construction and Mean-Field Theory of Quantum Spin Liquids

Quantum spin liquids (QSLs) are exotic magnetic phases that lack conventional long-range order even at zero temperature, typically arising in Mott insulators with strong quantum fluctuations. A theoretical route to describe QSLs involves representing the spin-$\frac{1}{2}$ degrees of freedom in terms of fermionic partons (Abrikosov fermions) [54, 55], which enables tractable mean-field descriptions.

Starting from the Hubbard model at half-filling:

$$H = \sum_{\langle ij\rangle} t_{ij}(c^{\dagger}_{\alpha i}c_{\alpha j} + \text{h.c.}) + U\sum_i n_{i\uparrow}n_{i\downarrow}, \tag{3.3}$$

in the strong interaction limit $U \gg t_{ij}$, the system becomes a Mott insulator, and low-energy physics is captured

by the Heisenberg model:

$$H = \sum_{\langle ij \rangle} J_{ij} \mathbf{S}_i \cdot \mathbf{S}_j, \quad \text{where } J_{ij} \sim \frac{t_{ij}^2}{U}. \tag{3.4}$$

The spin operator $\mathbf{S}_i$ can be rewritten using fermionic partons $f_{i\alpha}$ as:

$$\mathbf{S}_i = \frac{1}{2} f_{i\alpha}^\dagger \boldsymbol{\sigma}_{\alpha\beta} f_{i\beta}, \tag{3.5}$$

subject to the constraint $\sum_\alpha f_{i\alpha}^\dagger f_{i\alpha} = 1$ to project onto the physical Hilbert space.

Within the mean-field approximation, interaction terms are decoupled via hopping expectation values $\zeta_{ij} = \langle f_{i\alpha}^\dagger f_{j\alpha} \rangle$, and the single-occupancy constraint is enforced on average via a Lagrange multiplier $a_0(i)$. The resulting mean-field Hamiltonian reads:

$$H_{\text{MF}} = \sum_{\langle ij \rangle, \alpha} \left[ -\frac{1}{2} J_{ij} (f_{i\alpha}^\dagger f_{j\alpha} \zeta_{ij} + \text{h.c.}) - \frac{1}{2} J_{ij} |\zeta_{ij}|^2 \right] + \sum_{i,\alpha} a_0(i) (f_{i\alpha}^\dagger f_{i\alpha} - 1). \tag{3.6}$$

This mean-field theory describes spinons propagating in a self-consistent background and can realize various QSL phases depending on the pattern of $\zeta_{ij}$.

## 3.3 Exact Diagonalization(ED) and Density Matrix Renormalization (DMRG)

### 3.3.1 ED

To study quantum many-body systems, a key step involves solving the model Hamiltonian that governs their physical properties. This requires the computation of the eigenvalues and eigenvectors of the Hamiltonian operator [56]. The process begins by identifying the suitable basis that spans the Hilbert space of the system. Once the basis is defined, exploiting conserved quantities such as the total spin $S$ or its $z$-component $S^z$, becomes crucial in simplifying the problem. If the Hamiltonian commutes with a symmetry operator, such as $[H, S^z] = 0$, the Hamiltonian with full Hilbert space can be decomposed into smaller block diagonal form with invariant subspaces labeled by the conserved quantity. And each block diagonal matrices can be treated independently and thus drastically reduces the computational cost.

In a spin-$1/2$ system, each site has two states, $|\uparrow\rangle$ and $|\downarrow\rangle$, yielding a total Hilbert space dimension of $2^N$ for a system of $N$ spins. As this grows exponentially with system size, exact diagonalization is limited to relatively small systems (typically $N \lesssim 20$), even when symmetries are fully exploited.

The ED approach proceeds through the following key steps:

- Construction of basis states $|\psi_i\rangle$ for the chosen symmetry sector.
- Representation of the Hamiltonian as a matrix: $H_{ij} = \langle \psi_i | H | \psi_j \rangle$.
- Diagonalization of the resulting matrix to obtain eigenvalues and eigenvectors.

Since full diagonalization scales as $\mathcal{O}(m^3)$ (where $m$ is the Hilbert space dimension), it becomes extremely expensive for large $m$. To overcome this, iterative methods like the Lanczos algorithm [57, 58] and the Davidson method [59, 60] are employed to extract a few low-energy eigenstates efficiently, without constructing the full spectrum.

Despite its limitations in system size, ED remains a powerful tool for benchmarking other numerical techniques and obtaining qualitative insights into the ground state and low-energy excitations of quantum spin models.

### 3.3.2 DMRG

The Density Matrix Renormalization Group is a variational numerical technique introduced by White in 1992 [61], particularly well-suited for one-dimensional (1D) systems. It approximates the ground state by systematically optimizing a matrix product state (MPS) ansatz, which efficiently captures entanglement in 1D systems. Unlike ED, DMRG scales polynomially with system size, enabling simulations of hundreds of sites with high precision.

The DMRG algorithm works by iteratively growing the system and optimizing the wavefunction using reduced density matrices, truncating the less important basis states while retaining the most significant contributions to the entanglement. This makes it especially powerful for gapped 1D systems and ground state studies.

While DMRG is most accurate in 1D, it can be adapted to quasi-1D systems (e.g., ladders and cylinders) [62, 63]. Extensions to higher dimensions are possible but computationally demanding due to rapidly increasing entanglement.

## 3.4 Variational Monte Carlo

The *Variational Monte Carlo* (VMC) [64,65] method is a powerful computational approach used to study strongly correlated quantum systems. It combines the *quantum variational principle* with stochastic *Monte Carlo integration* to evaluate the expectation value of the Hamiltonian, starting from a trial wavefunction.

Given a Hamiltonian $H$ and a trial state $|\Phi\rangle$, the variational energy functional is defined as:

$$E[\Phi] = \langle\Phi|H|\Phi\rangle$$

According to the variational principle:

- $E_0 \leq E$, where $E_0$ is the true ground state energy of $H$,
- $E_0 = E$ if and only if $|\Phi\rangle = |\Psi_0\rangle$, the exact ground state.

The trial wavefunction $|\Psi\rangle$ typically depends on a set of variational parameters $\alpha_i$, which encode the physical correlations of the system. While in some special cases the parameters $\alpha_i$ can be derived analytically, most realistic systems, such as those involving Gutzwiller or Jastrow-type wavefunctions, require numerical treatment. Often, the wavefunction is constructed in real space:

$$\Psi_\alpha(r_{1\uparrow}, r_{2\uparrow}, \ldots, r_{N\uparrow})$$

where $r_{i\sigma}$ denote the coordinates of electrons with spin $\sigma$. A configuration $C \equiv (r_{1\uparrow}, r_{2\uparrow}, \ldots, r_{N\uparrow})$ thus defines a particular arrangement of particles.

The variational energy becomes:

$$E(\alpha_i) = \frac{\sum_C \Psi^*_\alpha(C) H \Psi_\alpha(C)}{\sum_C |\Psi_\alpha(C)|^2}$$

Since the number of configurations grows exponentially with system size (e.g., $\sim 2^{100}$ for 100 electrons), direct summation is infeasible. Instead, VMC samples configurations according to the probability distribution:

$$P(C) = \frac{|\Psi_\alpha(C)|^2}{\sum_C |\Psi_\alpha(C)|^2}$$

This allows us to express the energy as a statistical average over sampled configurations:

$$E(\alpha_i) = \sum_C P(C) \cdot \frac{H\Psi_\alpha(C)}{\Psi_\alpha(C)}$$

Using a Monte Carlo random walk through configuration space, VMC focuses computational effort on the most probable configurations, enabling accurate and efficient estimation of the variational energy.

# 4 Results

## 4.1 Project-I: Ab initio insights on the fermiology of $d^1$ transition metals on the honeycomb lattice: Hierarchy of hopping pathways and spin-orbit coupling

In this work [66], we investigate the low-energy electronic structure of $d^1$ honeycomb transition-metal halides of the form $MX_3$ (M = Ti, Zr, Hf; X = F, Cl, Br). These systems, with one electron in the $t_{2g}$ manifold, are promising candidates for exploring spin-orbital entangled physics and novel correlated metallic phases. Our primary objective is to establish a realistic tight-binding model grounded in first-principles calculations and to understand how the hierarchy of hopping amplitudes and spin-orbit coupling (SOC) determine the fermiology of these compounds.

Using density functional theory (DFT) and NMTO downfolding, we extract the effective hopping matrix elements between $t_{2g}$ orbitals and identify four symmetry-distinct types of nearest-neighbor hopping: direct $dd\sigma$, direct $dd\pi$, and two symmetry-allowed indirect hoppings, denoted by $ddm$ and $ddm'$[c.f Fig. 4]. The $dd\sigma$ term, which arises from strong direct orbital overlap, is found to dominate in most chlorides and bromides. This is a crucial deviation from the idealized SU(8) symmetric Dirac semimetal model, which assumes only indirect hoppings in the presence of strong SOC. The $ddm$ hopping term, mediated via ligand $p$-orbitals, plays a particularly important role in controlling the topological character of the band structure and even reverses sign in fluorides, placing them in a distinct regime of the phase diagram.

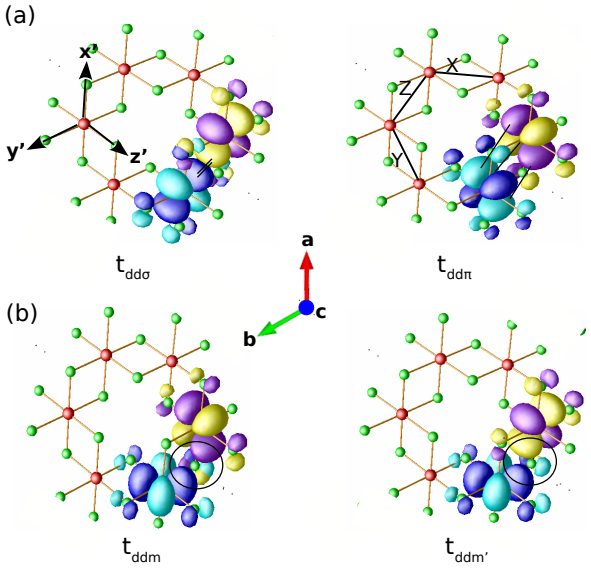


**Figure 4:** *Overlap of effective $t_{2g}$ Wannier functions in the downfolded basis of $ZrCl_3$, placed at two neighboring positions of Zr ions. Lobes of opposite signs are colored as blue (yellow) and cyan (violet) for two different Zr ions. (a) Direct dd overlaps, with left panel showing the head-on overlap ($dd\sigma$) and right panel showing the lateral overlap ($dd\pi$). The overlaps are highlighted by lines. The $t_{2g}$ orbitals are defined with the choice of local primed halogen-based coordinate systems, shown in left panel. The X, Y and Z M-M connecting bonds are shown in the right panel. The crystallographic coordinate system in terms of a, b and c is also shown. (b) Indirect overlaps via the halogen site, between the same (left) and differently shaped (right) $t_{2g}$ functions, labeled as ddm and ddm′ in the text. Overlap region via halogen is encircled*

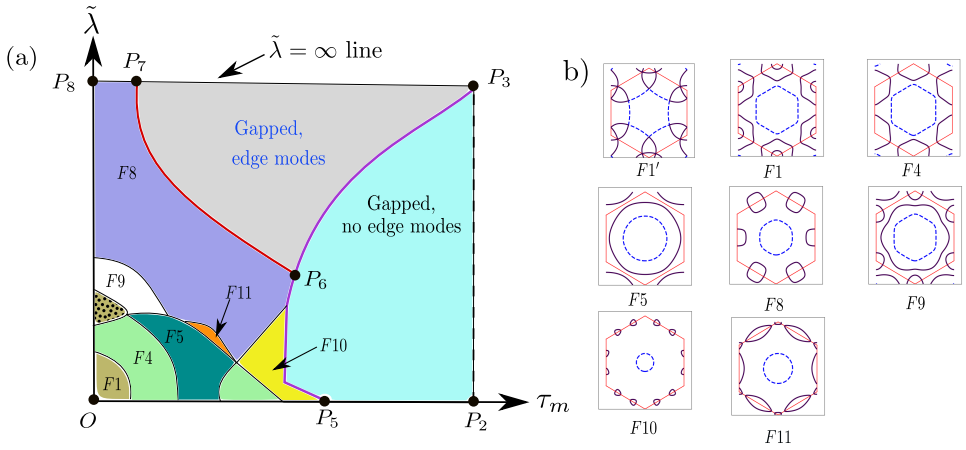


**Figure 5:** *(a) Phase diagram for $\rho = +1$ for Clorides and Bromides, $r = \frac{t_{dd\pi}}{t_{dd\sigma}} = -0.3$, $\tau'_m \propto t_{ddm'} = 0$. Two gapped phases shown in gray and cyan shading. The different metallic phases are shown with different colors and labeled as $F1$, …, $F11$. b) Fermi surfaces corresponding to different metallic phases. The hole-like Fermi surfaces are shown with blue dashed lines and the electron-like FS are shown with solid violet lines. The red line shows the boundary of the hexagonal BZ.*

The realistic tight-binding Hamiltonian, incorporating all four hopping channels and atomic SOC ($\lambda$), reveals a rich variety of electronic phases. In the idealized limit of strong SOC and indirect hopping, one obtains an SU(8) Dirac semimetal. However, with the inclusion of dominant $dd\sigma$ and subleading terms, the Dirac points generically gap out, yielding either a trivial or $\mathbb{Z}_2$ topological insulator. In practice, these insulating states are fragile and give way to compensated metallic phases due to residual band overlap. These metallic phases host small electron and hole pockets and are highly sensitive to the hopping ratio's value.

Of particular interest are the *Lifshitz transitions* that emerge in the fermiology. These are topological changes in the Fermi surface such as the creation, annihilation, or merging of Fermi pockets as one tunes the SOC strength or hopping ratios. For instance, in $ZrCl_3$ and $HfCl_3$, the materials lie close to a Lifshitz boundary separating different metallic phases (labeled $F_1$ through $F_{12}$) [c.f Fig 5]. In these regimes, even small external perturbations such as strain or pressure can induce qualitative changes in Fermi surface topology, potentially triggering instabilities like charge density waves or unconventional magnetic order.

To link theory with real materials, we develop a materials perspective phase diagram in the hopping-SOC parameter space [c.f. Fig 6]. This diagram maps different electronic regimes (trivial insulator, topological insulator, compensated metal) as functions of $t_{ddm}/t_{dd\sigma}$ and $\lambda/t_{dd\sigma}$. Real $MX_3$ compounds are then placed within this landscape based on DFT-derived parameters. Chlorides and bromides tend to cluster in the compensated metallic regions close to topological boundaries, while fluorides lie in a distinct quadrant where the sign of $ddm$ hopping changes. This mapping offers a practical guide for identifying materials close to critical points or phase boundaries, with high potential for tunable correlated phases.

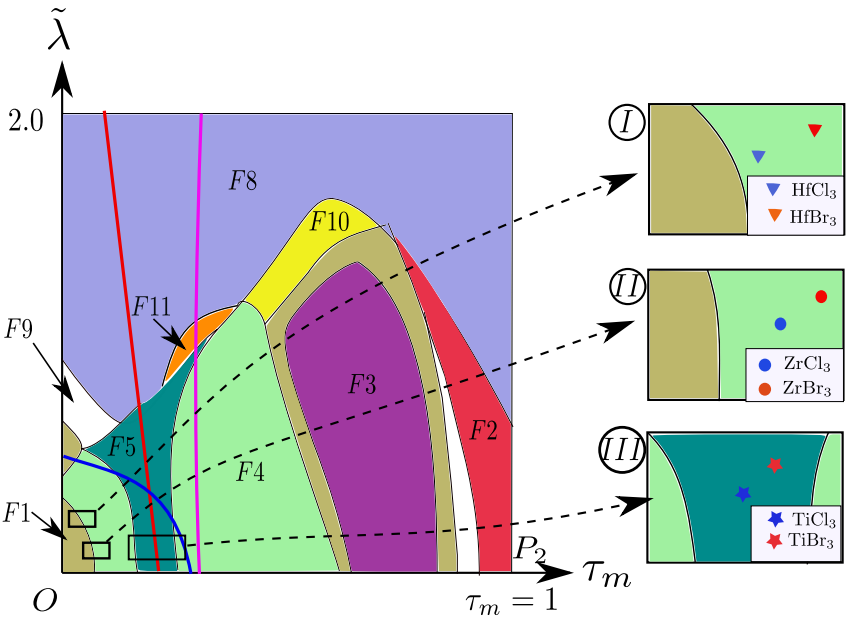


**Figure 6:** *Materials perspective phase diagram as a function of $t_{ddm}/t_{dd\sigma}$ and $\lambda/t_{dd\sigma}$, showing real $MX_3$ compounds superimposed on theoretical phase boundaries.*

In summary, this study demonstrates that the interplay of four types of hopping and SOC gives rise to a rich variety of low-energy behaviors in $d^1$ honeycomb halides. The presence of nearby Lifshitz transitions and material-tunable fermiology makes these systems a fertile ground for future exploration of interaction-driven phases such as spin-orbital liquids and unconventional density wave states.

## 4.2 Project-II: Multiple Dirac Spin-Orbital Liquids for SU(4) Heisenberg Antiferromagnets on Honeycomb Lattice

Quantum Spin Liquids (QSLs) represent an exotic phase of matter characterized by the absence of long-range magnetic order, despite strong electronic correlations. One of their hallmark features is the presence of fractionalized excitations. QSLs typically arise in systems where magnetic frustration prevents conventional ordering and enhances quantum fluctuations. This frustration can be geometric, as in the case of kagome or triangular lattices, or it can be due to the nature of the exchange interactions, such as in the Kitaev model [50].

An alternative and promising route to realizing QSLs is by enhancing the symmetry of the underlying spin Hamiltonian. In particular, SU(N) antiferromagnets have drawn attention because theoretical studies suggest that in the large-$N$ limit, these models can support non-trivial QSL phases even on bipartite lattices. Recent numerical work on the SU(4) antiferromagnetic Heisenberg model on the honeycomb lattice has provided evidence for the stabilization of a U(1) Dirac quantum spin liquid (D-QSL) [67].

However, the minimal model proposed by Yamada et al. [16], which includes only indirect (superexchange) hopping processes, may not fully capture the microscopic details of real materials such as $ZrCl_3$. Our first-principles calculations [66] in previous work reveal a rich hierarchy of hopping processes including direct $\sigma$-bonding ($t_\sigma$), $\pi$-bonding ($t_\pi$), and indirect (mediated) hopping ($t_m$), all of which are relevant in the broader $MX_3$ family of honeycomb lattice materials (see Fig. 7).

In this work, we start from a 4-orbital($J = 3/2$) Hubbard model incorporating these leading hopping amplitudes. In the strong coupling ($U/t >> 1$) and SOC ($\lambda \to \infty$) limit, derive the corresponding low-energy spin model. A key finding is that the space of hopping parameters naturally hosts several inequivalent SU(4) sub-manifolds. These include:

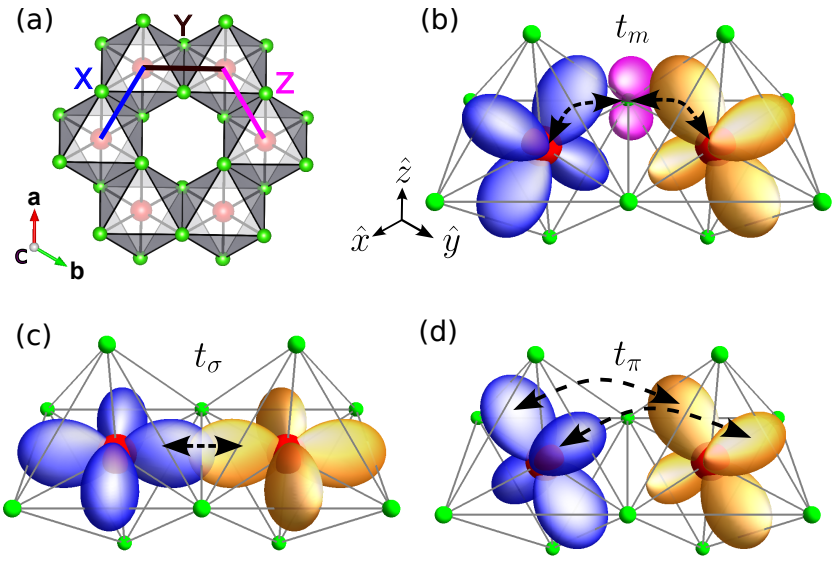


**Figure 7:** *Schematic representation of electronic hopping pathways in the honeycomb lattice of the compound* $MX_3$. *(a)* $MX_3$ *Honey comb lattice formed by the edge-shared*($MX_6$) *octahedra, where M and X atoms are represented by red and green spheres, respectively. (b) Indirect hopping pathways* ($t_m$)*, where neighboring transition metal (M) sites interact via an intervening halide (X) atom. (c) and (d) Direct d–d hopping pathways between* $t_{2g}$ *orbitals, showing head-on overlap* ($t_\sigma$) *and lateral overlap* ($t_\pi$)*, respectively.*

(i) $r = \frac{t_\pi}{t_\sigma} = 1$ limit,

(ii) Indirect hopping ($t_m$) only model, and

(iii) $r = \frac{t_\pi}{t_\sigma} = -\frac{1}{2}$ model.

Each of these limits realizes a distinct U(1) D-QSL, differing in the pattern of position-dependent SU(4) spin rotations. These spin rotations reflect different realizations of the microscopic symmetries and give rise to qualitatively different dynamical spin structure factors. Figure 8 presents the dynamical spin structure factor $S(\mathbf{q}, \omega)$ computed for these three limiting cases. The central panels show the energy-resolved spectral weight along a high-symmetry path in momentum space, while the side panels display constant-energy cuts within the Brillouin zone. Notably, these differing spin-liquid states leave distinct signatures in the momentum-energy structure of the spin response, making them amenable to experimental detection via neutron scattering or other spin-sensitive spectroscopic techniques.

These results highlight that the SU(4) D-QSL states, distinct from the one discussed by Yamada et al, may be more relevant for real materials like $ZrCl_3$, given the full set of hopping processes captured in the *ab initio* calculations.

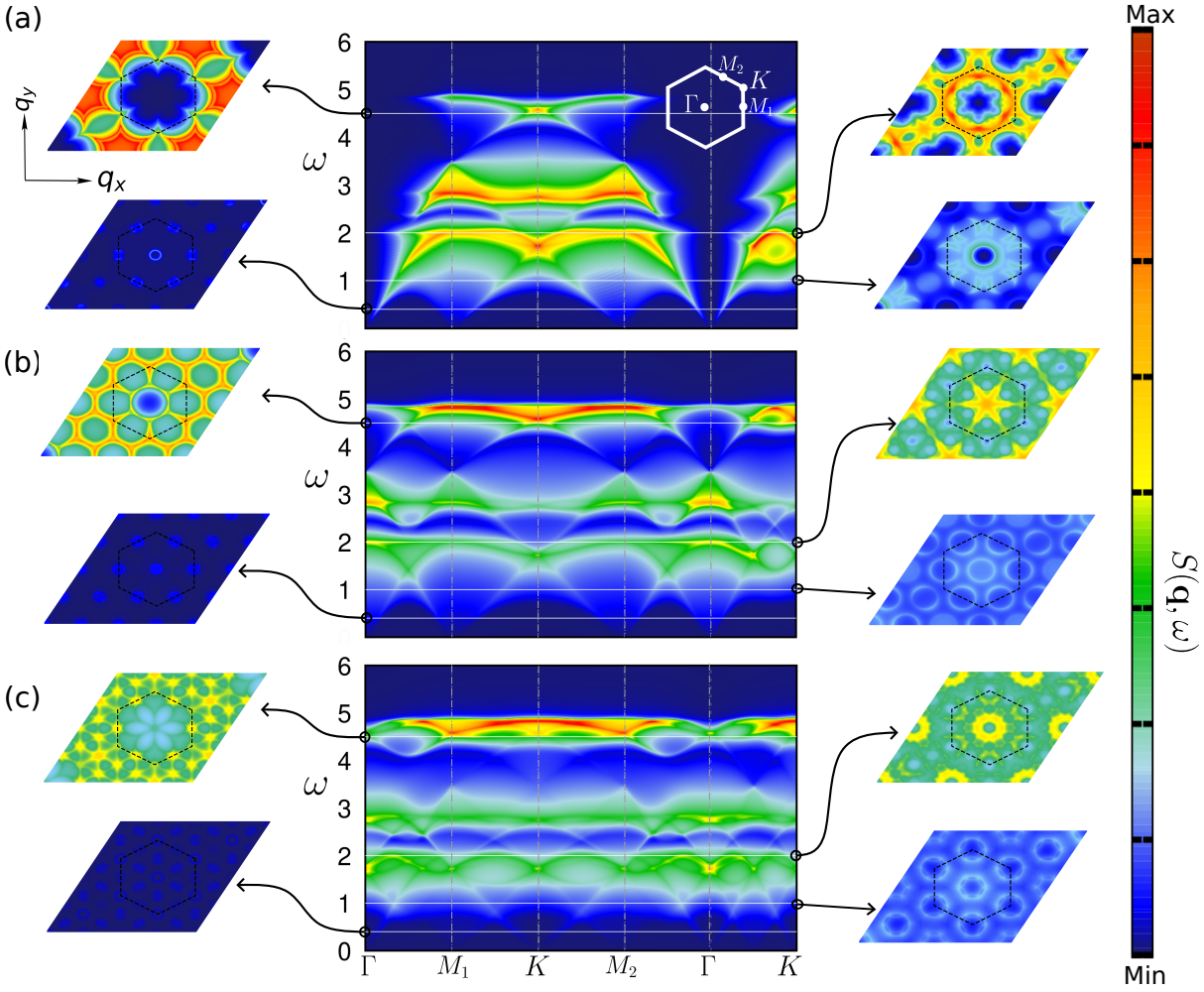


**Figure 8:** *Dynamical structure factor $S(\mathbf{q},\omega)$ in three limiting cases. Top, middle, and bottom rows correspond to the pure direct limit (a), indirect limit (b), and $r=-\frac{1}{2}$ limit (c), respectively. The middle column shows $S(\mathbf{q},\omega)$ as a function of energy $\omega$ (vertical axis) along the high-symmetry path $\Gamma$–$M_1$–$K$–$M_2$-$\Gamma$-$K$ in momentum space (horizontal axis). The color scale indicates intensity, with red (blue) denoting high (low) values. Left and right columns show constant-energy cuts of $S(\mathbf{q},\omega)$ in the $q_x$–$q_y$ plane; the first Brillouin zone is outlined by dotted black lines.*

## 4.3 Project-III: Interchain Interactions and Multimagnon Condensation in $NaVOPO_4$

One-dimensional (1D) spin-1/2 antiferromagnetic (AFM) chains are known to host rich quantum phenomena [44, 68,69] such as spin fractionalization, field-induced Bose-Einstein condensation (BEC), and magnetization plateaus. $NaVOPO_4$ is a vanadium-based spin-1/2 compound that crystallizes in a tetragonal lattice comprising chains of edge-sharing $VO_6$ octahedra. While early work described it as a nearly 1D Heisenberg chain compound with alternating AFM couplings $J$ and $J'$ mediated via $PO_4$ tetrahedra, its full three-dimensional (3D) spin model remained unclear. In this work, we address this by combining *ab initio* calculations with exact diagonalization to understand the role of interchain couplings, frustration, and strain in stabilizing an exotic multimagnon condensed phase. Using DFT and NMTO-downfolding, we construct a three-orbital low-energy model for the V $t_{2g}$ states and extract dominant hopping parameters. Four major hopping channels are identified [c.f Fig 9]: (1) $t$, (2) $t'$: strong AFM hoppings within the *ab*-plane via $PO_4$ units forming alternating spin chains, (3) $t_c$: a weak ferromagnetic hopping along the *c*-axis via $VO_6$ corner-sharing octahedra, and (4) $t_a$: an antiferromagnetic body-diagonal hopping. These hoppings are mapped onto a spin Hamiltonian comprising $J$, $J'$, $J_c$, and $J_a$. The signs and magnitudes of these couplings are confirmed via GGA+$U$ total energy mapping across multiple spin configurations.

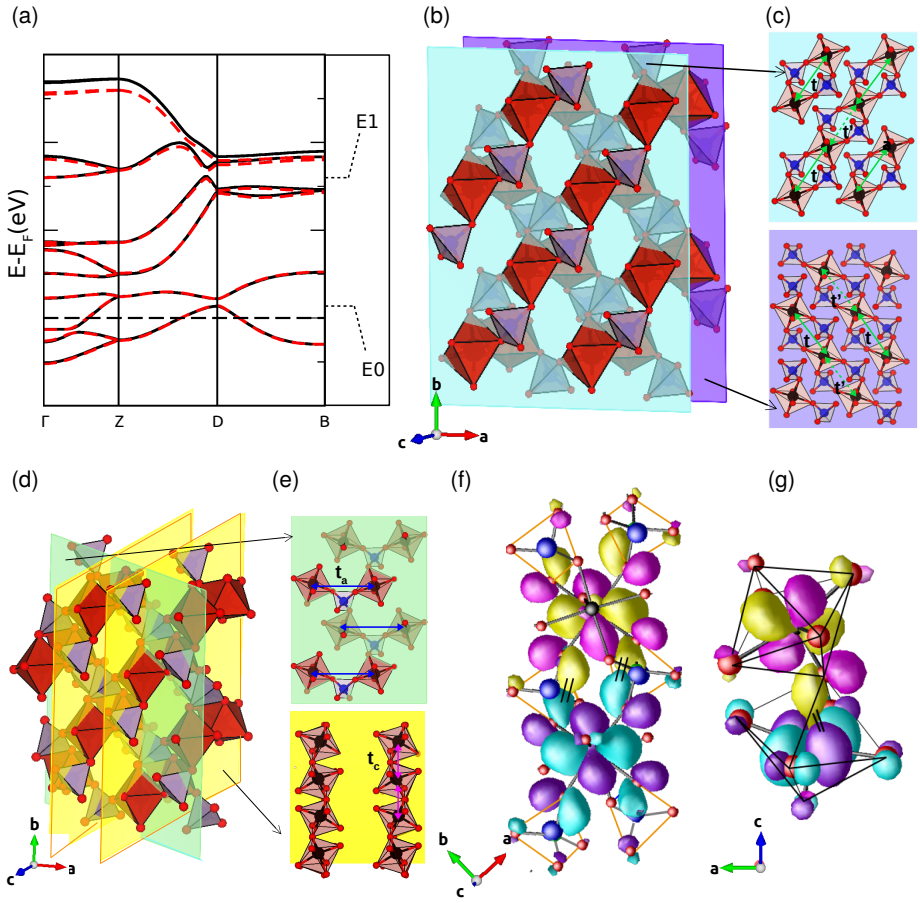


**Figure 9:** *Low-energy three-orbital model: (a) Downfolded bands (red) overlaid on DFT bands (black); (b–e) V–V hopping pathways $t$, $t'$, $t_c$, and $t_a$ across planes; (f–g) Isosurface plots of Wannier overlaps showing orbital symmetry and hopping channels.*

The 3D model is projected onto a 2D effective frustrated spin lattice with weakly alternating AFM chains (with $J'/J = 0.92$) and competing interchain couplings. We define an effective diagonal exchange $J_d = J_a + \gamma J_c$ to capture the body-diagonal effect of the FM interchain coupling $J_c$ and derive a $J_c/J$–$J_d/J$ phase diagram. This reveals three quantum phases:

- *Phase-I (Diagonal AFM):* Dominated by $J_d$, characterized by staggered diagonal AFM correlations.
- *Phase-II (Disordered):* A frustration-driven gapped quantum disordered state where $J_c \approx J_d$.
- *Phase-III (Stripy FM):* Dominated by $J_c$, favoring stripy ferromagnetic interchain correlations.

$NaVOPO_4$ is found to lie within or near the disordered region (Phase-II), consistent with prior experimental reports of a finite spin gap and lack of conventional long-range order. Applying an external magnetic field closes the spin gap and leads to a field-induced condensate. However, unlike standard magnon BEC observed in gapped dimer systems, we find that $NaVOPO_4$ exhibits a distinct *multimagnon condensation*. This is evidenced by magnetization jumps of $\Delta S^z > 1$ in exact diagonalization and the formation of tightly bound multimagnon states. The per-magnon binding energy becomes more negative with increasing field and system size, confirming the bound-state nature of the condensate.

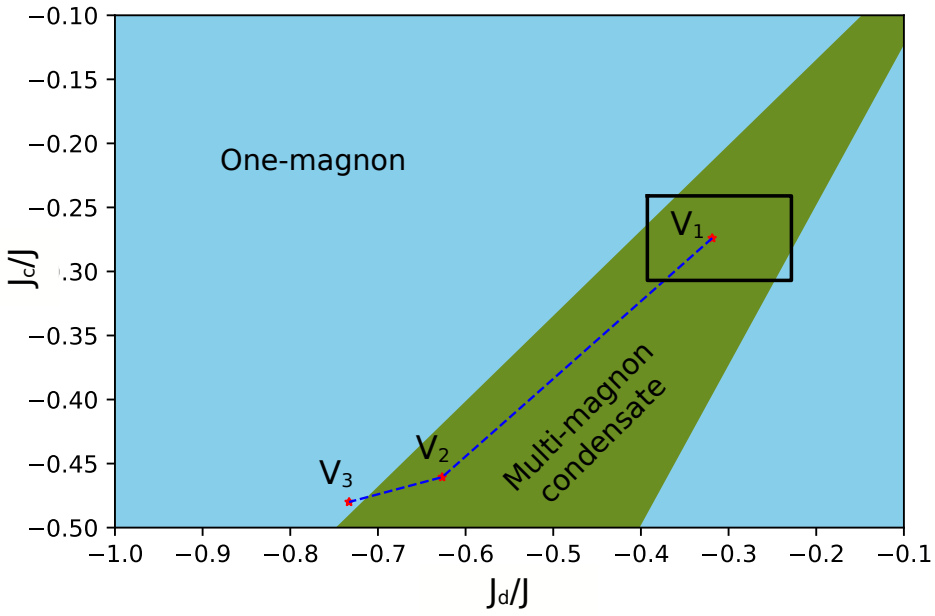


**Figure 10:** *Phase diagram in the $J_c/J$–$J_d/J$ space with $NaVOPO_4$ (red point) lying in the disordered multimagnon phase. dotted lines indicate strain tuning.*

We further study the effect of uniaxial tensile strain on magnetic interactions. A 1–3% elongation along the $c$-axis enhances both $J_c$ and $J_d$, pushing the system deeper into the disordered regime [c.f Fig 10]. This opens up the possibility of tuning $NaVOPO_4$ across a quantum critical point, allowing access to gapless critical behavior or long-range ordered states. The placement of $NaVOPO_4$ on the phase diagram suggests that it lies at a delicate balance point between competing couplings and is highly sensitive to external perturbations.

This work settles the long-standing question of interchain interactions in $NaVOPO_4$, identifies a novel multimagnon condensation mechanism, and proposes a route to tune its ground state via strain. The framework developed here is broadly applicable to other frustrated weakly dimerized spin-chain compounds and opens new directions for experimental exploration of field-induced and strain-controlled quantum phase transitions.

## 4.4 Project-IV: Role of topotactic hydrogen in Superconductivity of Infinite-layer Nickelate NdNiO2: A first-principles and variational Monte Carlo study

The emergence of superconductivity in infinite-layer nickelates such as $NdNiO_2$ has revived interest in cuprate-analog systems, with the added complexity of multiorbital physics and subtle structural sensitivities [33, 36]. One of the key open questions is the role of hydrogen, introduced during topotactic reduction via $CaH_2$, in tuning the electronic and superconducting behavior of these materials [70].

In this work, we investigate the microscopic impact of hydrogen incorporation on $NdNiO_2$ using a combined approach of density functional theory (DFT) and variational Monte Carlo (VMC). Our study focuses on interstitial hydrogen atoms residing near apical oxygen vacancies (AOVs), common in thin films post-reduction. While difficult to detect experimentally, recent Secondary-ion mass spectrometry (SIMS) studies confirm hydrogen's presence within the superconducting dome, motivating a theoretical study of its consequences.

Our DFT calculations show that hydrogen has a minimal effect on the Ni $d_{x^2-y^2}$ orbital, which dominates the low-energy states in undoped systems. However, the interstitial s-like (IS) orbital—centered near the AOV, experiences a significant change in spatial localization and energy. Specifically, the IS Wannier function becomes more localized near the Ni site bound to hydrogen, which alters its hybridization with neighboring orbitals. Figure 11 illustrates the orbital-resolved band structures for both hydrogenated and non-hydrogenated $NdNiO_2$. The IS orbital contribution near the Fermi level is significantly suppressed in the hydrogenated case, especially around the $k_z = \pi$ plane, where the electron pocket vanishes entirely.

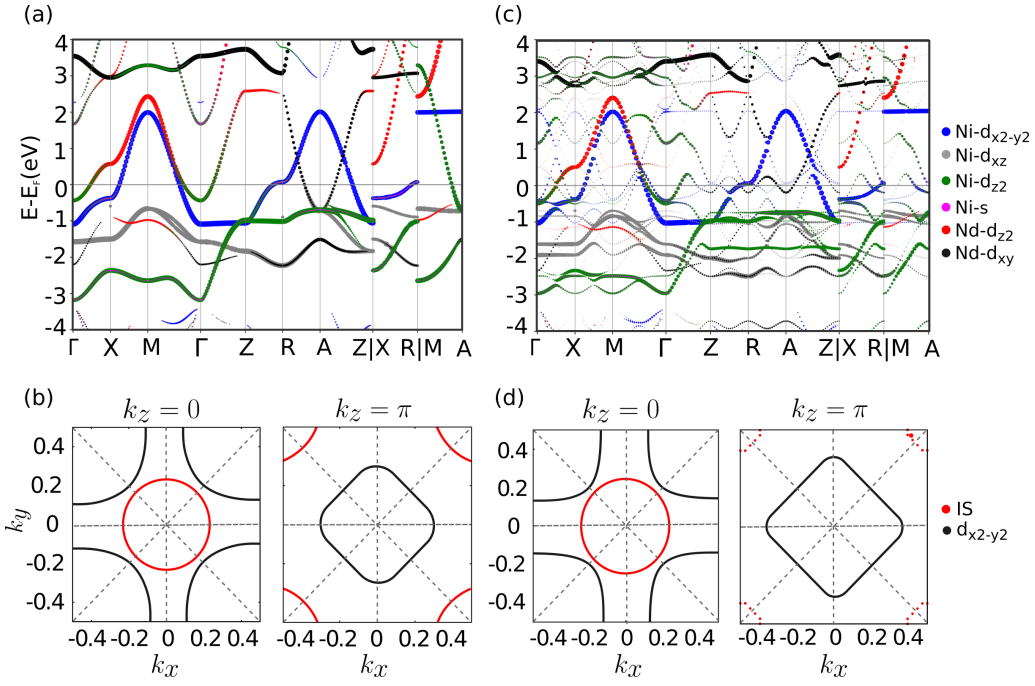


**Figure 11:** *(a) The GGA bandstructure of dehydrogenated $NdNiO_2$ compound, plotted along the high symmetry paths of the tetragonal BZ, Γ= (0,0,0), X = (π,0,0), M= (π,π,0), Z=(0,0,π), R = (π, 0, π), A= (π, π, π). The zero of the energy is fixed GGA Fermi energy and the bands was projected to Ni($d_{x^2-y^2}$, $d_{xy}$, $d_{z^2}$, $d_{xz}$, $d_{yz}$) and Nd($d_{z^2}$, $d_{xy}$) orbital characters. (b) The corresponding FS at $k_z = 0$ and $k_z = \pi$ planes. The contributions of $d_{x^2-y^2}$ (black) and IS (red) orbitals are marked. (c) Same as (a), but plotted for hydrogenated compound ($NdNiO_2H_{0.25}$). The bands are unfolded in the tetragonal BZ of $NdNiO_2$ to compare with the bandstructure of dehydrogenated compound. (d) Same as (b), plotted for $NdNiO_2H_{0.25}$.*

To assess the impact of this orbital rearrangement on superconductivity, we construct a two-orbital Hubbard model using the DFT-derived parameters and solve it using VMC. The wavefunction includes d-wave pairing on

the Ni $d_{x^2-y^2}$ orbital and s-wave pairing on the IS orbital—consistent with experimental indications of two-gap superconductivity in nickelates. The variational results reveal two distinct superconducting domes in the pairing amplitude versus carrier concentration. The first dome, dominated by IS orbital pairing, becomes more prominent with hydrogenation, while the second dome, driven by $d_{x^2-y^2}$ pairing, is only slightly suppressed.

These trends are captured in Figure 12, which shows the evolution of pairing order parameters with filling. Hydrogen enhances the IS channel by increasing the corresponding superexchange scale ($J_s \sim t_s^2/U_s$) due to stronger out-of-plane hopping. This orbital-selective enhancement supports the idea that hydrogen fine-tunes superconductivity rather than fundamentally enabling it.

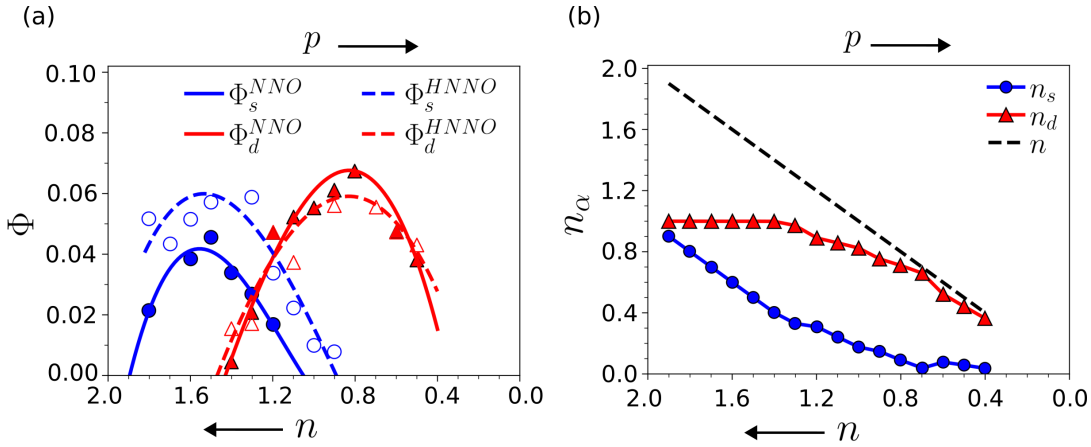


**Figure 12:** *(a) Superconducting order parameter, $\Phi_\alpha$ ($\alpha = d;\ s$) for hydrogenated $NdNiO_2$, compared to dehydrogenated $NdNiO_2$ as a function of electron density n. The open and closed symbols indicate VMC data corresponding to hydrogenated and dehydrogenated $NdNiO_2$, respectively. The solid and dashed lines are guide to eye corresponding to data points for hydrogenated and dehydrogenated $NdNiO_2$, respectively. (b) The orbital resolved electron density, $n_\alpha$ ($\alpha = d;\ s$) plotted as function of total electron density. The dashed line marks the fall of total electron density. The Hubbard interactions are fixed at $U_d = 3$ eV, $\frac{U_s}{U_d} = 0.5$ and $\frac{U_{sd}}{U_d} = 0.2$.*

Together, these findings suggest that the minimal low-energy physics of $NdNiO_2$ can still be captured by a two-orbital model even in the presence of hydrogen. Hydrogen modifies the balance between pairing channels without changing the overall topology of the Fermi surface or introducing new orbitals at the Fermi level. This provides a coherent explanation for why superconductivity persists in hydrogen-free films, while its robustness or $T_c$ may vary with hydrogen content.

In summary, our work reveals how subtle atomic-scale changes like the presence of topotactic hydrogen can reshape the electronic landscape and selectively enhance superconducting tendencies. By combining DFT and many-body techniques, we offer a material-specific, yet broadly applicable, picture of orbital-selective superconductivity in nickelates and related multiorbital systems.

# References


[1] Giniyat Khaliullin. Orbital order and fluctuations in mott insulators. *Progress of Theoretical Physics Supplement*, 160:155–202, 06 2005. doi:10.1143/PTPS.160.155.

[2] B. J. Kim, Hosub Jin, S. J. Moon, J.-Y. Kim, B.-G. Park, C. S. Leem, Jaejun Yu, T. W. Noh, C. Kim, S.-J. Oh, J.-H. Park, V. Durairaj, G. Cao, and E. Rotenberg. Novel $J_{\text{eff}} = 1/2$ mott state induced by relativistic spin-orbit coupling in $sr_2iro_4$. *Phys. Rev. Lett.*, 101:076402, Aug 2008. URL: https://link.aps.org/doi/10.1103/PhysRevLett.101.076402, doi:10.1103/PhysRevLett.101.076402.

[3] Lucile Savary and Leon Balents. Quantum spin liquids: a review. *Reports on Progress in Physics*, 80(1):016502, 2017. doi:10.1088/0034-4885/80/1/016502.

[4] Leon Balents. Spin liquids in frustrated magnets. *Nature*, 464(7286):199–208, 2010. doi:10.1038/nature08917.

[5] M. Z. Hasan and C. L. Kane. Colloquium: Topological insulators. *Rev. Mod. Phys.*, 82:3045–3067, Nov 2010. URL: https://link.aps.org/doi/10.1103/RevModPhys.82.3045, doi:10.1103/RevModPhys.82.3045.

[6] Xiao-Liang Qi and Shou-Cheng Zhang. Topological insulators and superconductors. *Rev. Mod. Phys.*, 83:1057–1110, Oct 2011. URL: https://link.aps.org/doi/10.1103/RevModPhys.83.1057, doi:10.1103/RevModPhys.83.1057.

[7] N. P. Armitage, E. J. Mele, and Ashvin Vishwanath. Weyl and dirac semimetals in three-dimensional solids. *Rev. Mod. Phys.*, 90:015001, Jan 2018. URL: https://link.aps.org/doi/10.1103/RevModPhys.90.015001, doi:10.1103/RevModPhys.90.015001.

[8] Ciarán Hickey and Arun Paramekanti. Thermal phase transitions of strongly correlated bosons with spin-orbit coupling. *Phys. Rev. Lett.*, 113:265302, Dec 2014. URL: https://link.aps.org/doi/10.1103/PhysRevLett.113.265302, doi:10.1103/PhysRevLett.113.265302.

[9] William Witczak-Krempa, Gang Chen, Yong Baek Kim, and Leon Balents. Correlated quantum phenomena in the strong spin-orbit regime. *arXiv preprint arXiv:1305.2193*, 2013. URL: https://doi.org/10.48550/arXiv.1305.2193.

[10] William Witczak-Krempa, Gang Chen, Yong Baek Kim, and Leon Balents. Correlated quantum phenomena in the strong spin-orbit regime. *Annual Review of Condensed Matter Physics*, 5(1):57–82, 2014. doi:10.1146/annurev-conmatphys-020911-125138.

[11] Leon Balents. Spin liquids in frustrated magnets. *Nature*, 464(7286):199–208, 2010. doi:10.1038/nature08917.

[12] G. Jackeli and G. Khaliullin. Mott insulators in the strong spin-orbit coupling limit: From heisenberg to a quantum compass and kitaev models. *Phys. Rev. Lett.*, 102:017205, Jan 2009. URL: https://link.aps.org/doi/10.1103/PhysRevLett.102.017205, doi:10.1103/PhysRevLett.102.017205.

[13] Masahiko G. Yamada, Masaki Oshikawa, and George Jackeli. Emergent SU(4) symmetry in $\alpha-zrcl_3$ and crystalline spin-orbital liquids. *Phys. Rev. Lett.*, 121:097201, Aug 2018. URL: https://link.aps.org/doi/10.1103/PhysRevLett.121.097201, doi:10.1103/PhysRevLett.121.097201.

[14] Yogesh Singh, S. Manni, J. Reuther, T. Berlijn, R. Thomale, W. Ku, S. Trebst, and P. Gegenwart. Relevance of the heisenberg-kitaev model for the honeycomb lattice iridates $A_2$iro$_3$. *Physical Review Letters*, 108:127203, 2012. doi:10.1103/PhysRevLett.108.127203.

[15] Arnab Banerjee, Paula Lampen-Kelley, Johannes Knolle, Christian Balz, Adam Anthony Aczel, Barry Winn, Yaohua Liu, Daniel Pajerowski, Jiaqiang Yan, Craig A. Bridges, Andrei T. Savici, Bryan C. Chakoumakos, Mark D. Lumsden, David Alan Tennant, Roderich Moessner, David G. Mandrus, and Stephen E. Nagler. Excitations in the field-induced quantum spin liquid state of $\alpha$-rucl$_3$. *npj Quantum Materials*, 3(8), 2018. URL: https://www.nature.com/articles/s41535-018-0079-2, doi:10.1038/s41535-018-0079-2.

[16] Masahiko G Yamada, Masaki Oshikawa, and George Jackeli. Emergent SU(4) symmetry in $\alpha$- ZrCl$_3$ and crystalline spin-orbital liquids. *Physical Review Letters*, 121(9):097201, 2018. URL: https://link.aps.org/doi/10.1103/PhysRevLett.121.097201, doi:10.1103/PhysRevLett.121.097201.

[17] Xiangang Wan, Ari M. Turner, Ashvin Vishwanath, and Sergey Y. Savrasov. Topological semimetal and fermi-arc surface states in the electronic structure of pyrochlore iridates. *Phys. Rev. B*, 83:205101, 2011. doi:10.1103/PhysRevB.83.205101.

[18] Stuart Calder, A. E. Taylor, Robert J. McQueeney, John Locker, Guang Cao, Ayman Said, and Jane Zhou. Magnetic and electronic properties of naoso$_3$ near its metal–insulator transition. *Phys. Rev. B*, 98:024432, 2018. doi:10.1103/PhysRevB.98.024432.

[19] D. Mandrus, A. J. Williams, B. C. Sales, B. Dabrowski, M. A. McGuire, and R. H. Friend. Continuous metal–insulator transition in the pyrochlore cd$_2$os$_2$o$_7$. *Phys. Rev. B*, 63:195104, 2001. doi:10.1103/PhysRevB.63.195104.

[20] Tai-Kai Ng and Patrick A. Lee. Mott insulator to superconductivity in sr$_2$vo$_4$. *Phys. Rev. B*, 64:165322, 2001. doi:10.1103/PhysRevB.64.165322.

[21] A. Krimmel, O. Janson, H. Rosner, V. Yushankhai, V. Tsurkan, J. Deisenhofer, and A. Loidl. Spin-orbital liquid – persistent dynamic correlations in the cubic spinel fesc$_2$s$_4$. *Phys. Rev. B*, 79:134406, 2009. doi:10.1103/PhysRevB.79.134406.

[22] Subhasish Mandal, Kristjan Haule, Karin M. Rabe, and David Vanderbilt. Electronic correlation in nearly free electron metals with beyond-dft methods. *npj Computational Materials*, 8(1):181, 2022. doi:10.1038/s41524-022-00867-8.

[23] Walter Kohn and Lu Jeu Sham. Self-consistent equations including exchange and correlation effects. *Physical Review*, 140(4A):A1133–A1138, 1965. doi:10.1103/PhysRev.140.A1133.

[24] Perdew, John P and Burke, Kieron and Ernzerhof, Matthias. Generalized gradient approximation made simple. *Physical review letters*, 77(18):3865, 1996. doi:10.1103/PhysRevLett.77.3865.

[25] Neil W. Ashcroft and N. David Mermin. *Solid State Physics*. Thomson Brooks/Cole, New York, 1976.

[26] Harald Ibach and Hans Lüth. *Solid-State Physics: An Introduction to Principles of Materials Science*. Springer, Berlin, 4 edition, 2010. doi:10.1007/978-3-642-03164-8.

[27] Daniel I. Khomskii. *Basic Aspects of the Quantum Theory of Solids: Order and Elementary Excitations*. Cambridge University Press, 2010.

[28] Pál Fazekas. *Lecture Notes on Electron Correlation and Magnetism*. World Scientific, 1999. doi:10.1142/2945.

[29] J. Bardeen, L. N. Cooper, and J. R. Schrieffer. Theory of superconductivity. *Physical Review*, 108:1175–1204, 1957. doi:10.1103/PhysRev.108.1175.

[30] J. G. Bednorz and K. A. Müller. Possible high $t_c$ superconductivity in the Ba–La–Cu–O system. *Zeitschrift für Physik B Condensed Matter*, 64:189–193, 1986. doi:10.1007/BF01303701.

[31] D. Vaknin, S. K. Sinha, D. E. Moncton, D. C. Johnston, J. M. Newsam, C. R. Safinya, and H. E. King. Antiferromagnetism in $La_2cuO_{4-y}$. *Physical Review Letters*, 58:2802–2805, 1987. doi:10.1103/PhysRevLett.58.2802.

[32] M. K. Wu, J. R. Ashburn, C. J. Torng, P. H. Hor, R. L. Meng, L. Gao, Z. J. Huang, Y. Q. Wang, and C. W. Chu. Superconductivity at 93 k in a new mixed-phase Y–Ba–Cu–O compound system at ambient pressure. *Physical Review Letters*, 58:908–910, 1987. doi:10.1103/PhysRevLett.58.908.

[33] D. Li, B. Y. Wang, K. G. Tak, G. D. Gu, and H. H. Wen. Superconductivity in an infinite-layer nickelate. *Nature*, 572:624–627, 2019. doi:10.1038/s41586-019-1649-8.

[34] J. Chaloupka and G. Khaliullin. Orbital order and possible superconductivity in $lanio_3$/$lamo_3$ superlattices. *Physical Review Letters*, 100:016404, 2008. doi:10.1103/PhysRevLett.100.016404.

[35] Q. Li, Y. H. Nie, M. K. Niranjan, and et al. Formation of conducting heterostructures from precisely layered $ndnio_3$/$ndalo_3$ superlattices. *Nanotechnology*, 22:534002, 2011. doi:10.1088/0957-4484/22/53/534002.

[36] Danfeng Li, Bai Yang Wang, Kyuho Lee, Shannon P. Harvey, Motoki Osada, Berit H. Goodge, Lena F. Kourkoutis, and Harold Y. H. Hwang. Superconducting dome in $nd_{1-x}sr_xnio_2$ infinite layer films. *Phys. Rev. Lett.*, 125:027001, 2020. doi:10.1103/PhysRevLett.125.027001.

[37] Ernst Ising. Beitrag zur theorie des ferromagnetismus. *Zeitschrift für Physik*, 31(1):253–258, 1925. doi:10.1007/BF02980577.

[38] Werner Heisenberg. Zur theorie des ferromagnetismus. *Zeitschrift für Physik*, 49:619–636, 1928. doi:10.1007/BF01328601.

[39] N. D. Mermin and H. Wagner. Absence of ferromagnetism or antiferromagnetism in one- or two-dimensional isotropic heisenberg models. *Physical Review Letters*, 17(22):1133–1136, 1966. doi:10.1103/PhysRevLett.17.1133.

[40] F. D. M. Haldane. Nonlinear field theory of large-spin heisenberg antiferromagnets: Semiclassically quantized solitons of the one-dimensional easy-axis néel state. *Physical Review Letters*, 50(15):1153–1156, 1983. doi:10.1103/PhysRevLett.50.1153.

[41] Mats Johnsson and Peter Lemmens. $Cute_2o_5$: A low-dimensional quantum magnet with spin dimers. *Chemistry of Materials*, 16(6):1046–1052, 2004. doi:10.1021/cm034906c.

[42] Helge Rosner, A. Kitaigorodsky, and W. E. Pickett. $Csv_2o_5$: A low-dimensional magnetic system with a large spin gap. *Physical Review Letters*, 88:186405, 2002. doi:10.1103/PhysRevLett.88.186405.

[43] M. Hase, I. Terasaki, and K. Uchinokura. Observation of the spin-peierls transition in linear $cu^{2+}$ (spin-1/2) chains in an inorganic compound $cugeo_3$. *Physical Review Letters*, 70(24):3651–3654, 1993. doi:10.1103/PhysRevLett.70.3651.

[44] Thierry Giamarchi, Christian Rüegg, and Oleg Tchernyshyov. Bose–einstein condensation in magnetic insulators. *Nature Physics*, 4:198–204, 2008. doi:10.1038/nphys893.

[45] Suchitra E. Sebastian, N. Harrison, C. D. Batista, L. Balicas, M. Jaime, P. A. Sharma, N. Kawashima, and I. R. Fisher. Dimensional reduction at a quantum critical point. *Nature*, 441:617–620, 2006. doi:10.1038/nature04745.

[46] Matthew B. Stone, Christopher D. Lumsden, Yiming Qiu, Edwin C. Samulon, Michael C. Shapiro, and Ian R. Fisher. Quasiparticle breakdown in a quantum spin liquid. *Physical Review Letters*, 100(23):237201, 2008. doi:10.1103/PhysRevLett.100.237201.

[47] Vivien S. Zapf, D. Zocco, B. R. Hansen, M. Jaime, N. Harrison, C. D. Batista, M. Kenzelmann, C. Niedermayer, A. Lacerda, and A. Paduan-Filho. Bose-einstein condensation of s = 1 nickel spin degrees of freedom in $nicl_2$-4sc$(nh_2)_2$. *Physical Review Letters*, 96(7):077204, 2006. doi:10.1103/PhysRevLett.96.077204.

[48] H. Takagi and T. Takayama. Control of spin-orbit entangled states in 4*d* and 5*d* transition metal oxides. *Journal of the Physical Society of Japan*, 89(1):012001, 2020.

[49] Tomohiro Takayama, Jiří Chaloupka, Andrew Smerald, Giniyat Khaliullin, and Hidenori Takagi. Spin–orbit-entangled electronic phases in 4d and 5d transition-metal compounds. *Journal of the Physical Society of Japan*, 90(6):062001, 2021. doi:10.7566/JPSJ.90.062001.

[50] Hidenori Takagi, Tomohiro Takayama, George Jackeli, Giniyat Khaliullin, and Stephen E Nagler. Concept and realization of Kitaev quantum spin liquids. *Nature Reviews Physics*, 1(4):264–280, 2019. doi:10.1038/s42254-019-0038-2.

[51] J. B. Marston and I. Affleck. Large-*n* limit of the hubbard-heisenberg model. *Physical Review B*, 39(16):11538–11558, 1989. doi:10.1103/PhysRevB.39.11538.

[52] P. Hohenberg and W. Kohn. Inhomogeneous electron gas. *Physical Review*, 136(3B):B864–B871, 1964. doi:10.1103/PhysRev.136.B864.

[53] Jianwei Sun, Adrienn Ruzsinszky, and John P. Perdew. Strongly constrained and appropriately normed semilocal density functional. *Physical Review Letters*, 115(3):036402, 2015. doi:10.1103/PhysRevLett.115.036402.

[54] G. Baskaran, Z. Zou, and P. W. Anderson. The resonating valence bond state and high-$T_c$ superconductivity—a mean field theory. *Solid State Communications*, 63(11):973–976, 1987. doi:10.1016/0038-1098(87)90642-9.

[55] G. Baskaran and P. W. Anderson. Gauge theory of high-temperature superconductors and strongly correlated fermi systems. *Physical Review B*, 37(1):580–583, 1988. URL: https://journals.aps.org/prb/abstract/10.1103/PhysRevB.37.580, doi:10.1103/PhysRevB.37.580.

[56] Giuseppe Grosso and Giuseppe P. Parravicini. *Solid State Physics*. Academic Press, Amsterdam, 2nd edition, 2014. URL: https://www.sciencedirect.com/book/9780123850300/solid-state-physics.

[57] Cornelius Lanczos. An iteration method for the solution of the eigenvalue problem of linear differential and integral operators. *Journal of Research of the National Bureau of Standards*, 45(4):255–282, 1950. doi:10.6028/jres.045.026.

[58] Cornelius Lanczos. Solution of systems of linear equations by minimized iterations. *Journal of Research of the National Bureau of Standards*, 49(1):33–53, 1952. doi:10.6028/jres.049.006.

[59] Ernest R. Davidson. The iterative calculation of a few of the lowest eigenvalues and corresponding eigenvectors of large real-symmetric matrices. *Journal of Computational Physics*, 17(1):87–94, 1975. doi:10.1016/0021-9991(75)90065-0.

[60] Ernest R. Davidson and W. J. Thompson. Monster matrices: their eigenvalues and eigenvectors. *Computers in Physics*, 7(5):519–522, 1993. doi:10.1063/1.4823120.

[61] Steven R. White. Density matrix formulation for quantum renormalization groups. *Physical Review Letters*, 69(19):2863–2866, 1992. doi:10.1103/PhysRevLett.69.2863.

[62] Ulrich Schollwöck. The density-matrix renormalization group. *Reviews of Modern Physics*, 77(1):259–315, 2005. doi:10.1103/RevModPhys.77.259.

[63] E. M. Stoudenmire and S. R. White. Studying two-dimensional systems with the density matrix renormalization group. *Annual Review of Condensed Matter Physics*, 3(1):111–128, 2012. doi:10.1146/annurev-conmatphys-020911-125018.

[64] W. M. C. Foulkes, L. Mitas, R. J. Needs, and G. Rajagopal. Quantum monte carlo simulations of solids. *Reviews of Modern Physics*, 73(1):33–83, 2001. doi:10.1103/RevModPhys.73.33.

[65] D. M. Ceperley, G. V. Chester, and M. H. Kalos. Monte carlo simulation of a many-fermion study. *Physical Review B*, 16(7):3081–3099, 1977. doi:10.1103/PhysRevB.16.3081.

[66] Manoj Gupta, Basudeb Mondal, Subhro Bhattacharjee, and Tanusri Saha Dasgupta. Ab initio insights on the fermiology of $d^1$ transition metals on the honeycomb lattice: Hierarchy of hopping pathways and spin-orbit coupling. *Phys. Rev. Res.*, 5:043219, Dec 2023. URL: https://link.aps.org/doi/10.1103/PhysRevResearch.5.043219, doi:10.1103/PhysRevResearch.5.043219.

[67] Gang Cao and Lance E Delong. *Frontiers of 4D-and 5D-transition Metal Oxides*. World Scientific, 2013.

[68] El abadila Iffer, Mohammed Belaiche, Chouaib Ahmani Ferdi, Moustapha Elansary, Abdul Khader Sunar, Yanxia Wang, and Yuliang Cao. Monoclinic -navopo4 as cathode materials for sodium-ions batteries: Experimental and dft investigation. *International Journal of Energy Research*, 45(2):1703–1719, 2021. URL: https://onlinelibrary.wiley.com/doi/abs/10.1002/er.5835, arXiv:https://onlinelibrary.wiley.com/doi/pdf/10.1002/er.5835, doi:10.1002/er.5835.

[69] Prashanta K. Mukharjee, K. M. Ranjith, B. Koo, J. Sichelschmidt, M. Baenitz, Y. Skourski, Y. Inagaki, Y. Furukawa, A. A. Tsirlin, and R. Nath. Bose-einstein condensation of triplons close to the quantum critical point in the quasi-one-dimensional spin-$\frac{1}{2}$ antiferromagnet $NaVOPO_4$. *Phys. Rev. B*, 100:144433, Oct 2019. URL: https://link.aps.org/doi/10.1103/PhysRevB.100.144433, doi:10.1103/PhysRevB.100.144433.

[70] Javier Gainza, Carlos A. López, Federico Serrano-Sánchez, João Elias F.S. Rodrigues, Angelika D. Rosa, María Isabel Sobrados, Norbert M. Nemes, Neven Biskup, María T. Fernández-Díaz, José Luis Martínez,

and José Antonio Alonso. Evidence of hydrogen content and monovalent Ni oxidation state in non-superconducting bulk anchored infinite-layer nickelates. *Cell Reports Physical Science*, 4(12):101724, 2023. URL: https://www.sciencedirect.com/science/article/pii/S2666386423005696, doi:10.1016/j.xcrp.2023.101724.